Cobalt complexes of an OSNSO-tetrapodal pentadentate ligand: Synthesis, structures and reactivity

Lucas Thevenin, Jean-Claude Daran, Rinaldo Poli, Christophe Fliedel

Cobalt complexes of an OSNSO-tetrapodal pentadentate ligand: Synthesis, structures and reactivity.

Lucas Thevenin[a], Jean-Claude Daran[a], Rinaldo Poli*[a], Christophe Fliedel*[a]

[a] LCC-CNRS, Université de Toulouse, CNRS, INPT, Toulouse, France
* Corresponding authors. E-mail address: christophe.fliedel@lcc-toulouse.fr (C. Fliedel), rinaldo.poli@lcc-toulouse.fr (R. Poli).

Dedicated to Maurizio Peruzzini on the occasion of his 65th birthday.

Abstract

The novel pentadentate tetrapodal proligand 2,6-bis[(2-hydroxyphenyl)sulfanylmethyl]pyridine (**1**·H_2) and its cobalt(II) complex [Co(**1**)] (**2**) were synthesized and characterized by several analytical (EA, ESI-MS) and spectroscopic methods (NMR or EPR, FT-IR), including X-ray crystallography for **1**·H_2. Cyclic voltammetry studies showed that **2** undergoes a reversible metal-based oxidation (Co^{II}/Co^{III}). Complex **2** was designed to be applied to organometallic mediated radical polymerization (OMRP), however it exhibited an extremely poor solubility in non-coordinating solvents and several vinyl monomers (styrene, vinyl acetate and *tert*-butyl acrylate), which hampers its potential as moderator. Complex **2** has a high affinity towards Lewis bases, such as pyridine, leading to the clean formation of the mono-pyridine adduct **2**·py, as confirmed by X-ray crystallography. In **2**·py, ligand **1** is pentacoordinated to the Co^{II} center, with the two thioether-phenolate (S,O) moieties oriented *anti* to each other, and the only free coordination site of the octahedron is completed by the additional pyridine, *trans* to the central pyridine linker of **1**. The equilibrium between **2** and **2**·py could be studied by ^{1}H NMR. Complex **2** could be cleanly and quantitatively oxidized to its diamagnetic iodo cobalt(III) analog [Co(**1**)I] (**3**), by simple reaction with iodine. The latter could then be subjected to a halide abstraction reaction, mediated by K[$B(C_6F_5)$], affording the cationic complex [Co(**1**)][$B(C_6F_5)$], **4**.

Highlights

- Cobalt(II) complexes of a bis(thioether)-bis(phenolato)-pyridyl-based OSNSO-ligand.
- Neutral (OSNSO)-cobalt(III) iodide and cationic (OSNSO)-cobalt(III) complexes.
- XRD, NMR, CV and EPR studies.
- Evaluation in radical polymerization.

Graphical abstract

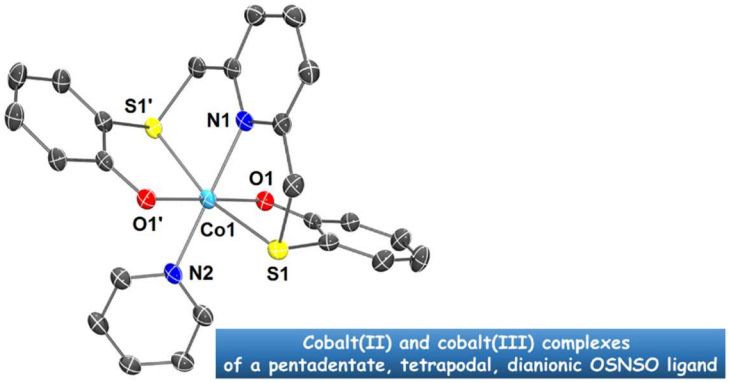

Keywords

Cobalt complexes; Bis(phenolato) ligands; Thioether ligands; Salen analogues; Crystal structures; NMR

Introduction

Transition metal catalysis is an essential tool in many fields, such as the synthesis of fine chemicals, natural products and pharmaceuticals. While this area has been dominated by catalysts based on noble metals such as Pd, Pt, Rh and Ir, it is now urgent to replace them by catalysts derived from non-precious metals, such as Mn, Fe and Ni, which are less-expensive, more abundant and sustainable and sometimes less-toxic [1, 2]. Iron and cobalt complexes are now well established as efficient (pre)catalysts for many transformations [1-3], particularly hydrogenation reactions [4-6].

Another important field of application of iron and cobalt complexes is polymer synthesis, particularly by metal-mediated radical polymerization. While iron complexes are gaining more and more attention in atom transfer radical polymerization (ATRP) [7-9] as an alternative to copper catalysts for the above-mentioned reasons, cobalt complexes are the compounds of choice to mediate organometallic mediated radical polymerization (OMRP) [10-16]. Both techniques of controlled radical polymerization make use of a transition metal complex ([L/Mt]), available in two successive oxidation states (x and x+1), as moderator to control the active/propagating radical species ($P^{\bullet}$) concentration, thereby favoring a controlled chain growth and limiting undesired (irreversible) termination reactions (Scheme 1) [17-20]. However, ATRP and OMRP differ by the way in which the complex operates during the process. While the low valent metal complex ([L/Mt^{x}]) acts as activator of the halogen-capped dormant chain (P-Y) in ATRP, leading to the active radical species ($P^{\bullet}$) and the deactivator ([L/Mt^{x+1}-Y]), it serves as deactivator in OMRP, via direct carbon/polymer-metal bond formation, resulting in an organometallic dormant species ([L/Mt^{x+1}-P], Scheme 1).

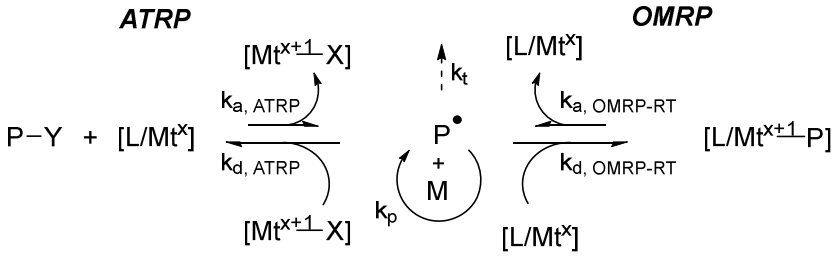

Scheme 1. ATRP (left), OMRP (right) equilibria. M = monomer, [L/Mt] = transition metal complex, x and x+1 = oxidation states, P_n = propagating polymer chain, Y = halogen.

Recently, we focused our attention on the development of iron-based moderating systems for the ATRP of reactive monomers such as methyl methacrylate (MMA) [21-23], and on manganese- [24, 25] and cobalt-based systems [26-33] for the OMRP of less activated monomers (LAMs = monomers leading to poorly stabilized radicals) such as vinyl acetate (VAc) or vinylidene fluoride (VDF).

The common point for the development of more efficient systems, both for fine chemicals or polymeric materials production, relies on the understanding of the reaction mechanisms and the relationship between the catalysts structure and its activity [34, 35]. Over the last decade, our group has highlighted, through both experimental and computational investigations, how subtle changes in the complex/ligand architecture may affect its performances in radical polymerization [36-39].

Several ligands have already been evaluated in Co-mediated OMRP. It was recently shown that the ligand structure and the nature of the donor set, such as N_4 (porphyrin-type), N_2O_2 (salen-type) and $(O_2)_2$ (acac-type), influences the equilibrium constant of the moderating processes [34]. Therefore, in the present study, we designed a new pentadentate tetrapodal ligand, inspired by salen/salalen/salan ligands in which the N donor is replaced by a S (thioether) donor and incorporating a capping pyridine donor (Figure 1). Such a combination of donor atoms was only reported once, for the synthesis of a copper(II) complex, as model of the active site of the enzyme galactose oxidase [40]. The OSNSO-

cobalt(II) complex isolated after coordination presents only one coordination site available for radical coordination under OMRP condition, and should therefore avoid the contribution of any other phenomena (monomer chelation, coordinating solvent interaction…) to the OMRP equilibrium [41]. Accessibility of this coordination site and of the +III oxidation state were investigated by paramagnetic ^{1}H NMR spectroscopy and cyclic voltammetry, respectively.

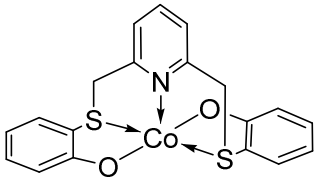

Figure 1. Representation of the targeted cobalt(II) complex, supported by the newly developped pentadentate tetrapodal OSNSO ligand.

1. Experimental procedures

1.1. General considerations

Only the polymerization tests and the synthesis of complex **2** were carried out under inert atmosphere (Ar), in flame-dried glassware and with dried and/or distilled monomers and solvents (see below). All other operations were carried out in air and using non-dried glassware and solvents.

1.2. Materials

Compounds cobalt(II) acetylacetonate (Acros Organics, 99%), potassium tetrakis pentafluorophenyl borate (Alfa Aesar, 99%), 2,6-bis(hydroxymethyl)pyridine (Sigma Aldrich, 98%), 2-mercaptophenol (Acros Organics, 98+%), iodine (Acros Organics, 99.5%), pyridine (Acros Organics, 99+%), sodium hydroxide (Carlo Erba, 97%), 2,2'-Azobis(4-methoxy-2.4-dimethyl valeronitrile) (V-70, Wako Chemicals), azobisisobutyronitrile (AIBN, Sigma Aldrich, 98%), 2,2,6,6-tetramethyl-1-piperidinyloxy (TEMPO, Acros Organics, 98%), mesitylene (Sigma Aldrich, >99.9 %), d_6-DMSO (99.8%D, Euriso-top), d_5-pyridine (99.5%D, Euriso-top), CD_2Cl_2 (99.9%D, Euriso-top) and $CDCl_3$ (99.8%D, Euriso-top) were used as received, without prior purification. Laboratory Reagent grade (≥99.5%) ethanol, dichloromethane, acetone, pentane and methanol were purchased from VWR Chemicals and used as received, without prior purification. Toluene and THF were dried using an MBraun SPS system. Vinyl acetate (VAc, >99 %, Sigma Aldrich), *tert*-butyl acrylate (tBa, Sigma Aldrich, 98%) and styrene (St, Sigma Aldrich, >99%) were dried over calcium hydride, distilled under argon, degassed by several freeze/pump/thaw cycles and stored under argon. 2,6-bis(chloromethyl)pyridine was prepared following a previously reported procedure [42].

1.3. Instrumentation

The NMR spectra were recorded on a Bruker Avance III 300 or 400 MHz spectrometer at ambient temperature. ^{1}H and ^{13}C chemical shifts (δ) are reported in ppm *vs*. $SiMe_4$ and were determined by reference to the residual ^{1}H and ^{13}C solvent peaks. The coupling constants are reported in Hertz. The IR spectra were recorded in the 4000−100 cm^{-1} region on a PerkinElmer Frontier FT-IR spectrometer (ATR mode, diamond crystal). The electrospray mass spectra (ESI-MS) were recorded on a Q-Tof Premier (Waters) instrument using nitrogen as drying agent and nebulizing gas and MeCN as solvent. The elemental analyses for all compounds were carried out by the analytical service of the LCC-Toulouse using a PerkinElmer 2400 CHNS/O Series II System (100V). Voltammetric measurements were carried out with an Autolab PGSTAT100 potentiostat. Experiments were performed at room temperature in a homemade airtight three–electrode cell connected to a vacuum/argon line. The

reference electrode consisted of a saturated calomel electrode (SCE) separated from the solution by a bridge compartment. The counter electrode was a platinum wire of ca 1cm² apparent surface. The working electrode was a Pt microdisk (0.5 mm diameter). The supporting electrolyte [^{n}Bu$_4$N][PF$_6$] (Fluka, 99% puriss electrochemical grade) was used as received and simply degassed under argon. Dichloromethane was purified under nitrogen atmosphere using solvent purification equipment (MBraun) prior to use. The solutions used during the electrochemical studies were typically 10^{-3} M in complex compound and 0.1 M in supporting electrolyte. Before each measurement, the solutions were degassed by bubbling Ar and the working electrode was polished with a polishing machine (Presi P230). Compound **2** was very poorly soluble in dichloromethane, however the addition of pyridine (8 µL in 10 mL of DCM) improved the solubility, supposedly promoting the formation of compound **2**·py. The EPR spectrum was obtained at 4.13 K on an Elexsys E 500 Bruker spectrometer, operating at a microwave frequency of approximately 9.5 GHz, using a microwave power of 20 mW across a sweep width of 150 mT (centered at 310 mT) with modulation amplitude of 0.5 mT. UV-Visible spectra were recorded on a PerkinElmer Lambda 35 spectrophotometer, using a quartz Hellma Analytics high precision cell with a light path of 10 mm.

1.4. X-ray structural analyses

A single crystal of each compound was mounted under inert perfluoropolyether at the tip of a glass fiber and cooled in the cryostream of either a Rigaku Oxford Diffraction GEMINI EOS diffractometer for **2**·py or a Bruker Nonius APEXII diffractometer for **1**·H$_2$. The structures were solved by direct methods (SHELXt) [43] and refined by least-squares procedures on F^2 using SHELXL-2014 [44]. All H atoms attached to carbon were introduced in the calculations in idealized positions and treated as riding models. In compound **2**·py, the unit cell contains a certain amount of pentane. These pentane molecules appear to be highly disordered and it was difficult to model their positions and distribution reliably. Therefore, the SQUEEZE function of PLATON [45] was used to eliminate the contribution of the electron density in the solvent region from the intensity data, and the solvent-free model was employed from the final refinement. The drawing of the molecules was realized with the help of ORTEP32 [46, 47] and POV-Ray version 3.7. Crystal data and refinement parameters are shown in Table 1. Selected distances and angles are reported below Figures 1 and 3. All bond lengths and angles (Tables S1 and S2) and hydrogen interactions (Table S3) are given in the ESI.

Crystallographic data have been deposited with the Cambridge Crystallographic Data Centre as supplementary publication no. 2034822-2034823. Copies of the data can be obtained free of charge on application to the Director, CCDC, 12 Union Road, Cambridge CB2 1EZ, UK (fax: (+44) 1223-336-033; e-mail: deposit@ccdc.cam.ac.uk).

Table 1. Crystal data for **1**·H$_2$ and **2**·py.

Identification code	**1**·H$_2$ (CCDC 2034822)	**2**·py (CCDC 2034823)
Empirical formula	$C_{19}H_{17}NO_2S_2$	$C_{24}H_{20}CoN_2O_2S_2$
Formula weight	355.45	491.46
Temperature, K	173(2)	173.2(3)
Wavelength, Å	0.71073	1.54184
Crystal system	Monoclinic	Orthorhombic
Space group	$P2_1/n$	Pbcn
a, Å	9.5890(5)	7.8069(4)
b, Å	9.1824(5)	15.4402(7)
c, Å	19.2580(11)	22.4263(12)
α, °	90.0	90.0
β, °	92.262(2)	90.0
γ, °	90.0	90.0

Volume, Å^3	1694.35(16)	2703.3(2)
Z	4	4
Density (calc), Mg/m^3	1.393	1.208
Abs. coefficient, mm^{-1}	0.325	6.579
F(000)	744	1012
Crystal size, mm^3	0.470 x 0.180 x 0.120	0.45 x 0.38 x 0.16
Theta range, °	2.412 to 30.033	3.942 to 61.541
Reflections collected	13224	5418
Indpt reflections (R_{int})	4910 (0.0225)	2066 (0.0405)
Completeness, %	99.1	96.2
Absorption correction	Multi-scan	Multi-scan
Max. / min. transmission	0.7471 and 0.6759	1.0 and 0.252
Refinement method	F^2	F^2
Data /restraints/parameters	4910 / 0 / 219	2066 / 0 / 143
Goodness-of-fit on F^2	1.052	1.080
R1, wR2 [I>2σ(I)]	0.0333, 0.0988	0.0701, 0.1822
R1, wR2 (all data)	0.0409, 0.1046	0.0813, 0.1908
Residual density, e.Å^{-3}	0.418 / -0.280	0.934 / -0.569

1.5. Synthesis of pro-ligand **1**·H_2

Pure 2-mercaptophenol (4.51 g, 3.6 mL, 35.8 mmol, 2 eq) was slowly added to a solution of 2,6-di(chloromethyl)pyridine (3.15 g, 17.9 mmol, 1 eq) in 180 mL of deoxygenated ethanol. Sodium hydroxide (1.43 g, 35.8 mmol, 2 eq) and water (18 mL) were then added and the resulting solution was stirred overnight at room temperature. The resulting colorless precipitate was isolated by filtration and dried under reduced pressure. Recrystallization from an acetone/H_2O mixture afforded **1**·H_2 as colorless needles (5.15 g, 81% yield). Anal. Calcd for $C_{19}H_{17}NO_2S_2$ (355.47): C, 64.20; H, 4.82; N, 3.94; S, 18.04%. Found: C, 63.88; H, 4.66; N, 3.94; S, 17.61%. MS (ESI): *m/z* 356.0 $[M + H]^+$. FTIR: ν_{max}(solid)/cm^{-1}: 3480br, 3137br, 1593m, 1574m, 1492w, 1467s, 1453s, 1401m, 1356w, 1293s, 1251s, 1223w, 1217w, 1173m, 1152s, 1027m, 1011m, 945w, 938w, 888m, 865m, 834m, 808m, 753vs, 732sh, 713m, 677m, 611m. ^{1}H NMR (400 MHz, d_6-DMSO): δ (ppm) 4.21 (4H, s, CH_2), 6.71 (2H, dt, ^3J = 7.6 Hz, ^4J = 1.2 Hz, H_{arom}), 6.84 (2H, dd, ^3J = 8.0 Hz, ^4J = 1.6 Hz, H_{arom}), 7.04 (2H, dt, ^3J = 8.0 Hz, ^4J = 1.6 Hz, H_{arom}), 7.20 (2H, dd, ^3J = 8.0 Hz, ^4J = 1.6 Hz, H_{arom}), 7.25 (2H, d, ^3J = 7.6 Hz, H_{arom}), 7.69 (1H, t, ^3J = 8.0 Hz, H_{arom}), 9.98 (2H, s, br, OH). ^{13}C{^{1}H} NMR (101 MHz, d_6-DMSO): δ (ppm) 37.5 (CH_2), 115.5 (CH_{arom}), 120.0 (CH_{arom}), 121.8 (C_{quat}), 122.1 (CH_{arom}), 128.0 (CH_{arom}), 130.4 (CH_{arom}), 138.7 (CH_{arom}), 155.9 (C_{quat}), 157.3 (C_{quat}).

1.6. Synthesis of complex **2**

Under inert atmosphere, solid $[Co(acac)_2]$ (1.40 g, 5 mmol) was added to a stirred toluene (15 mL) solution of pro-ligand **1**·H_2 (1.93 g, 5 mmol) at 0°C. The resulting solution was allowed to warm up at room temperature and further heated at 90°C overnight, leading to the formation of a yellow precipitate. The reaction mixture was cooled down to room temperature and the pale yellow solid was filtered off and dried under vacuum (1.53 g, 75% yield). Anal. Calcd for $C_{19}H_{15}CoNO_2S_2$ (412.39): C, 55.34; H, 3.67; N, 3.40%. Found: C, 55.10; H, 3.65; N, 3.60%. MS (ESI): *m/z* 413.0 $[M + H]^+$, 430.0 $[M + NH_4]^+$. FTIR: ν_{max}(solid)/cm^{-1}: 1595m, 1579s, 1557w, 1513w, 1463vs, 1455sh, 1435s, 1409m, 1312vs, 1287m, 1261m, 1238m, 1156w, 1126w, 1094w, 1029w, 1014w, 901w, 852m, 838s, 796m, 770s, 740vs, 721m, 700w, 676w, 601w, 576sh, 567m, 525s, 477m, 463m, 409s. CV: see main text and ESI.

1.7. Synthesis of complex **2**·py

Complex **2** (50 mg, 0.12 mmol) was dissolved in pyridine (8 mL) at room temperature to afford a yellow solution, which was stirred overnight at room temperature. Addition of pentane (20 mL) induced precipitation of the pyridine adduct **2**·py, which was isolated as a light brown powder after decanting off the mother liquor, further washing with pentane (2 x 10 mL) and drying under vacuum (56.6 mg, 95% yield). Anal. Calcd for $C_{24}H_{20}CoN_2O_2S_2$ (491.49): C, 58.65; H, 4.10; N, 5.70; S, 13.05%. Found: C, 57.56; H, 3.67; N, 5.87; S, 12.07%. MS (ESI): *m/z* 514.0 $[M + Na]^+$, 412.0 $[M - py]^+$. FTIR: ν_{max}(solid)/cm^{-1}: 1594m, 1578s, 1556w, 1545w, 1460vs, 1452sh, 1435s, 1408w, 1311vs, 1286m, 1260m, 1238m, 1156w, 1147w, 1125w, 1094w, 1029m, 1013m, 958w, 944w, 918w, 901m, 882w, 852m, 838s, 796m, 769s, 740vs, 721m, 700m, 676m, 600m, 577m, 566m, 526s, 476m, 463m, 408s. ^{1}H NMR (400 MHz, d_5-pyridine): δ (ppm) 69.1 (width = 48.5 Hz, s, 1H), 65.8 (61.2 Hz, s, 1H), 52.8 (22.2 Hz, s, 1H), 47.4 (22.2 Hz, s, 1H), 10.3 (57.7 Hz, s, 13H, py), 8.9 (16.4 Hz, s, 7H, py), 8.6 (32.5 Hz, s, 13H, py), 7.3 (21.0 Hz, s, 2H), 5.1 (29.1 Hz, s, 1H), -4.7 (17.6 Hz, s, 1H). EPR: see main text and ESI. UV-Vis: λ_{max}(pyridine)/nm: 413 (ε/dm^3 mol^{-1} cm^{-1}: 1 210).

1.8. Synthesis of complex **3**

Solid I_2 (90 mg, 0.39 mmol, 0.5 eq) was added all at once to a stirred suspension of complex **2** (320 mg, 0.77 mmol, 1 eq) in 10 mL of methanol at room temperature. The resulting mixture was stirred at room temperature overnight. A dark brown precipitate formed and was isolated by filtration. The latter was then washed with pentane (3 x 10 mL) and dried under vacuum, affording a dark brown solid (315 mg, 77% yield). Anal. Calcd for $C_{19}H_{15}CoINO_2S_2$ (539.29): C, 42.32; H, 2.80; N, 2.60; S, 11.89%. Found: C, 42.55; H 2.55; N, 2.75; S, 11.89%. MS (ESI): *m/z* 412.0 $[M - I]^+$. FTIR: ν_{max}(solid)/cm^{-1}: 1598w, 1576s, 1549m, 1462s, 1452vs, 1442sh, 1390w, 1377m, 1321sh, 1306s, 1269s, 1239m, 1184w, 1165w, 1156w, 1124m, 1092m, 1048w, 1033w, 1022m, 976w, 932w, 882m, 849s, 783m, 749s, 740vs, 701m, 677m, 644m, 606w, 579m, 536w, 465s, 434s, 416sh. ^{1}H NMR (300 MHz, d_6-DMSO): δ (ppm) 5.12 (4H, d, ^4J = 6.1 Hz, CH_2), 6.46 (2H, d, ^3J = 8.4 Hz, H_{arom}), 6.56 (2H, pseudo t, ^3J = 7.4 Hz, H_{arom}), 6.85 (2H, pseudo t, ^3J = 7.7 Hz, H_{arom}), 7.60 (2H, d, ^3J = 7.7 Hz, H_{arom}), 7.79 (1H, d, ^3J = 7.4 Hz, H_{arom}), 7.82 (2H, d, ^3J = 8.4 Hz, H_{arom}). ^{1}H NMR (400 MHz, $CDCl_3$): δ (ppm) 4.73 and 5.19 (4H, AX spin system, ^2J = 16 Hz, CH_2), 6.64 (4H, m, H_{arom}), 6.92 (2H, pseudo t, ^3J = 7.6 Hz, H_{arom}), 7.39 (2H, d, ^3J = 7.6 Hz, H_{arom}), 7.62 (1H, pseudo t, ^3J = 7.6 Hz, H_{arom}), 7.67 (2H, d, ^3J = 6.8 Hz, H_{arom}). $^{13}C\{^1H\}$ NMR (101 MHz, d_6-DMSO): δ (ppm) 55.6 (CH_2), 113.6 (C_{quat}), 115.5 (CH_{arom}), 120.1 (CH_{arom}), 122.2 (CH_{arom}), 130.4 (CH_{arom}), 131.4 (CH_{arom}), 138.5 (CH_{arom}, para-*N*), 159.6 (C_{quat}), 173.8 (C_{quat}). UV-Vis: λ_{max}(CH_2Cl_2)/nm: 417 (ε/dm^3 mol^{-1} cm^{-1}: 2 440), 535sh.

1.9. Synthesis of complex **4**

A CH_2Cl_2 solution (1 mL) of K[B(C_6F_5)] (22 mg, 30.6 µmol, 1 eq) was added dropwise to a stirred CH_2Cl_2 solution (3 mL) of complex **3** (16.5 mg, 30.6 µmol, 1 eq) at room temperature, and the resulting mixture was stirred for 16 h. After evaporation to dryness, washing with pentane (2 x 5 mL) and drying under vacuum, a dark powder was isolated (33.4 mg, 90% yield). Anal. Calcd for $C_{43}H_{15}BCoF_{20}NO_2S_2$ (1091.43): C, 47.32; H, 1.39; N, 1.28%. Found: C, 47.47; H, 1.62; N, 1.17%. MS (ESI): *m/z* 412.0 $[M - B(C_6F_5)]^+$. FTIR: ν_{max}(solid)/cm^{-1}: 1644w, 1578w, 1514m, 1456vs, 1397sh, 1373w, 1303w, 1266m, 1241sh, 1083s, 975vs, 885w, 851w, 774m, 768sh, 755s, 725w, 683m, 661m, 610w, 601w, 573m, 465w, 438m. ^{1}H NMR (300 MHz, d_6-acetone): δ (ppm) 5.02 (4H, s, CH_2), 6.42 (2H, d, ^3J = 8.4 Hz, H_{arom}), 6.54 (2H, pseudo t, ^3J = 7.5 Hz, H_{arom}), 6.86 (2H, pseudo t, ^3J = 7.8 Hz, H_{arom}), 7.70 (4H, d, ^3J = 7.5 Hz, H_{arom}), 7.91 (1H, t, ^3J = 7.8 Hz, H_{arom}). $^{19}F\{^1H\}$ NMR (282 MHz, d_6-acetone): δ (ppm) -133.0 (d), -164.4 (t), -168.0 (t). $^{11}B\{^1H\}$ NMR (128 MHz, d_6-acetone): δ (ppm) = -16.6. UV-Vis: λ_{max}(CH_2Cl_2)/nm: 401 (ε/dm^3 mol^{-1} cm^{-1}: 1 700).

1.10. Polymerization tests

All polymerization tests were carried out in bulk monomer or with addition of pyridine, under a protective argon atmosphere, in flame-dried glassware and using distilled and degassed monomers.

As a representative procedure, a Schlenk tube equipped with a magnetic stirrer was charged with the cobalt complex (**2** or **2**·py, 1 equiv.), freshly distilled monomer (St, tBA, VAc, 100-1000 equiv.), pyridine in some cases (see main text) and 0.3 mL of mesitylene as internal reference. The mixture was degassed by three freeze/pump/thaw cycles. The initiator (V-70 for tests at 30°C or AIBN for tests at 65 and 80°C, 0.6 equiv. in all cases) was added under an argon flow on the top of the frozen mixture before the last pump cycle. The Schlenk tube was immersed in an oil bath at the desired temperature (starting time t_0). Whenever samples were withdrawn during the polymerization, they were collected under an argon flow by a syringe followed by quenching of the polymerization by adding TEMPO. Conversions were determined by ^{1}H NMR.

2. Results and discussion

2.1. Synthesis and characterization of the OSNSO pro-ligand **1**·H_2

Pro-ligand **1**·H_2 was synthesized in two steps with a global yield of 64%. In a first step, commercially available 2,6-bis(hydroxymethyl)pyridine was converted into 2,6-bis(chloromethyl)pyridine, in 79% yield, using thionyl chloride in dry THF, following a previously reported procedure [42]. Reaction between 2,6-bis(chloromethyl)pyridine and 2 equiv. of commercially available 2-hydroxythiophenol in the presence sodium hydroxide (2 equiv.) afforded the desired pro-ligand **1**·H_2 in 81% yield after recrystallization from an acetone/H_2O mixture (Scheme 2) [40]. The latter was characterized by elemental analysis (EA), by mass spectrometry (ESI-MS), and by infrared (FT-IR) and multi-nuclear NMR spectroscopic techniques (see Exp. Section). Both ^{1}H and ^{13}C{^{1}H} NMR spectra of **1**·H_2 are consistent with the ligand C_2-symmetry (see ESI – Figures S1 and S2), *e.g.* only one signal for the equivalent *meta*-H pyridine or CH_2 linkers, and the most intense peak in the ESI mass spectrum, with m/z = 356, correspond to $[M + H]^+$.

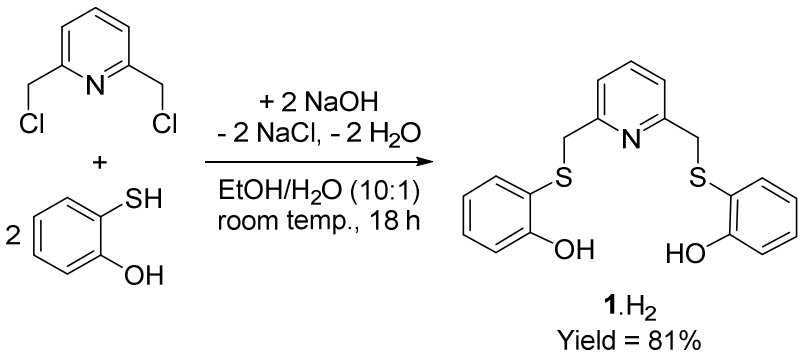

Scheme 2. Synthesis of the OSNSO pro-ligand **1**·H_2.

The X-ray diffraction analysis of a single crystal grown by diffusion of water into a saturated solution of **1**·H_2 in acetone confirmed its structure, as depicted in Figure 2. Compound **1**·H_2 crystallizes in the monoclinic $P2_1/n$ space group with four independent molecules in the unit cell. The phenol O2-H group is involved as proton donor in an H-bond with the proton acceptor pyridine N1 atom [N1•••O2 2.708(1) Å] and, at the same time, as proton acceptor towards the second phenol O1-H moiety [O1•••O2 2.808(1) Å] (see ESI – Table S3). No X-ray structures of free (pro)ligands presenting the OSNSO skeleton are available for comparison. However, the structural parameters of **1**·H_2 may be compared with those of related compounds incorporating the characteristic aryl 2-picolyl thioether scaffold [48-51]. In particular, both CH_2-S (aver. 1.825 Å) and C_{arom}-S (aver. 1.774 Å) bond lengths and the CH_2-S-C_{arom} angles (99.2° and 103.2°) in **1**·H_2 are in the same ranges found for the aforementioned compounds, i.e. CH_2-S [1.804(2)-1.835(18) Å], C_{arom}-S [1.759(4)-1.779(4) Å] and CH_2-S-C_{arom} [99.91(8)-105.05(9)°] (see ESI – Table S1 for the list of bond lengths and angles for **1**·H_2) [48-51].

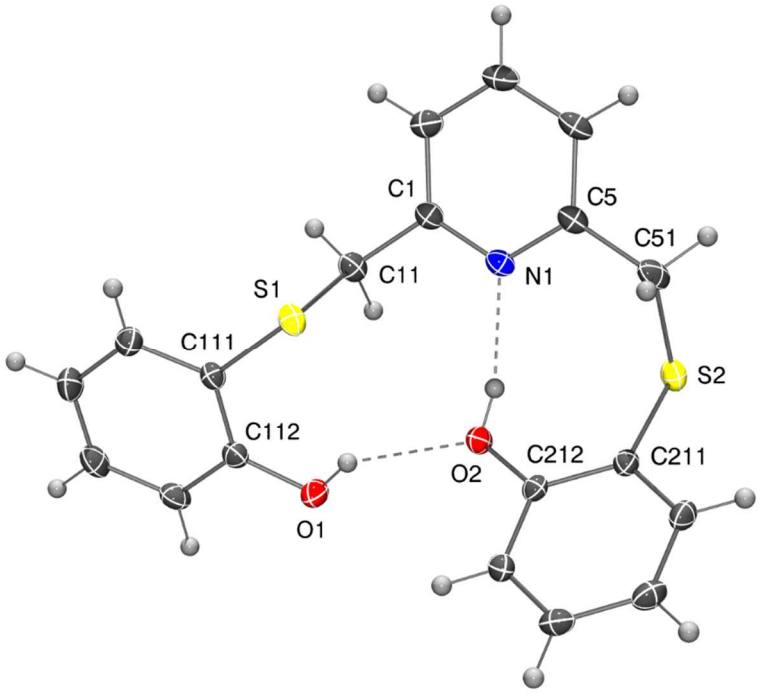

Figure 2. View of the molecular structure of **1**·H_2 with ellipsoids set at the 50% probability level. H atoms are represented as small spheres of arbitrary radii. Hydrogen bond interactions are represented as dashed bond. Selected bond lengths (Å) and angles (deg.): N1-C1 1.3455(16), N1-C5 1.3425(15), O1-C112 1.3597(14), S1-C111 1.7707(12), S1-C11 1.8298(13), O2-C212 1.3589(13), S2-C211 1.7770(12), S2-C51 1.8189(13), C11-S1-C111 99.17(6), C51-S2-C211 103.16(6).

2.2. Synthesis and characterization of cobalt(II) complexes (2 and 2·py)

The neutral OSNSO-cobalt(II) complex **2** was synthesized in good yield (75%) by reaction between pro-ligand **1**·H_2 and an equimolar amount of [Co(acac)$_2$], acting both as metal source and base. Complex **2** is extremely poorly soluble in non-coordinating solvents, however its composition could be confirmed by EA and ESI-MS. The latter spectrum revealed the $[M + H]^+$ ion (m/z = 413.0) as the most intense peak, with the expected isotopic distribution (see ESI – Figure S3). Alternatively, complex **2** could be synthesized by reaction between pro-ligand **1**·H_2, $CoCl_2$ and NEt_3 in a 1:1:3.3 molar ratio, but the yield of this reaction was lower (30%) and the procedure more time consuming (separation of **2** from the ammonium salt). Unfortunately, all attempts to obtain single crystals of **2** were unsuccessful. The low solubility of **2** in non-coordinating solvents such as chloroform or dichloromethane did not allow to obtain spectroscopic information in such solvents. On the other hand, the addition of increasing amounts of pyridine to **2** in CD_2Cl_2 led to increased solubility and to the appearance of paramagnetically shifted resonances in the ^{1}H NMR spectrum, which continuously shifted as a function of the py/Co ratio, as shown in Figure 3. This observation suggests the coordination of one pyridine molecule to complex **2**, favoring its dissolution by stabilization of a mononuclear form (Scheme 3). Indeed, the structure of **2** is most likely dimeric with a diphenoxide-bridged bioctahedral geometry, as previously established for several other related compounds (see e.g. [52-57]). There are, however, no examples of dinuclear cobalt(II) compounds with an O_3NS_2 coordination environment in the Cambridge Structural Database.

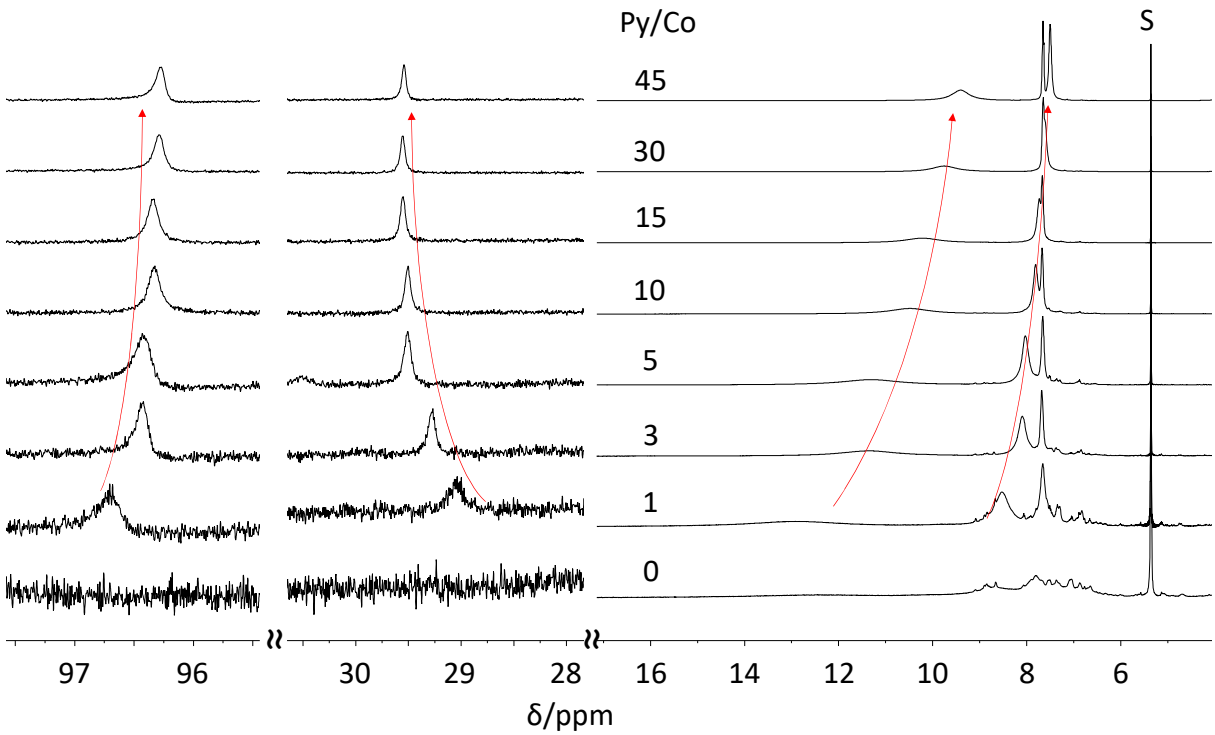

Figure 3. ^{1}H NMR spectra obtained for complex **2** in CD_2Cl_2 in the presence of variable amounts of pyridine. The resonance marked with S is the solvent resonance.

Only one average resonance for each type of proton was observed at all pyridine concentrations, showing that the coordination/decoordination process (equation 1) is fast on the NMR timescale. Therefore, the observed position of each signal depends on the chemical shift values of all species involved in the equilibrium and on their relative concentrations, which depend on the equilibrium constant. The resonances of the coordinated ligand (**1**), equilibrating between two paramagnetic complexes, converged at high [py] to the resonances of the adduct, [Co(**1**)(py)] or **2**·py, whereas the resonances of pyridine, equilibrating between the paramagnetic **2**·py complex and the diamagnetic free ligand, converged at high [py] toward the resonances of free pyridine. Besides the three pyridine resonances (*o*, *m* and *p* protons in a 2:2:1 ratio), the intensities of which grew proportionally to py/Co, only two additional resonances attributable to the OSNSO ligand were clearly visible at δ ca. 96 and 29 in a 1:1 ratio, thus their structural assignment is uncertain. The chemical shift dependence of four resonances (marked with red arrows in Figure 3), two of ligand **1** and two of pyridine, could be analyzed as a function of the py/Co ratio in order to extract the equilibrium constant of the ligand addition process (equation 1). The *p*-py resonance could not be used for this purpose because its chemical shift is insensitive to the py/Co ratio (δ = 7.65 ppm).

$$[Co(\mathbf{1})]_2 + 2\ py \rightleftharpoons 2\ [Co(\mathbf{1})(py)] \qquad (1)$$

The equations and the procedure used for the data fitting are described in the ESI. It is worth noting that, in case the pyridine-free complex (**2**) is a pentacoordinated mononuclear species, different equations and a simpler procedure for the data fitting would apply. This model, the full description of which is also available in the ESI, gave results of slightly lower quality. For the dinuclear model, all four independent fits gave an equilibrium constant in a narrow range, for an average K = 32.8±3.3, whereas the mononuclear model yielded constants in a different range from the data fitting of the ligand and pyridine resonances, for an overall average K = 58±19. This analysis is therefore in support of the dinuclear structural assignment to **2** (Scheme 3).

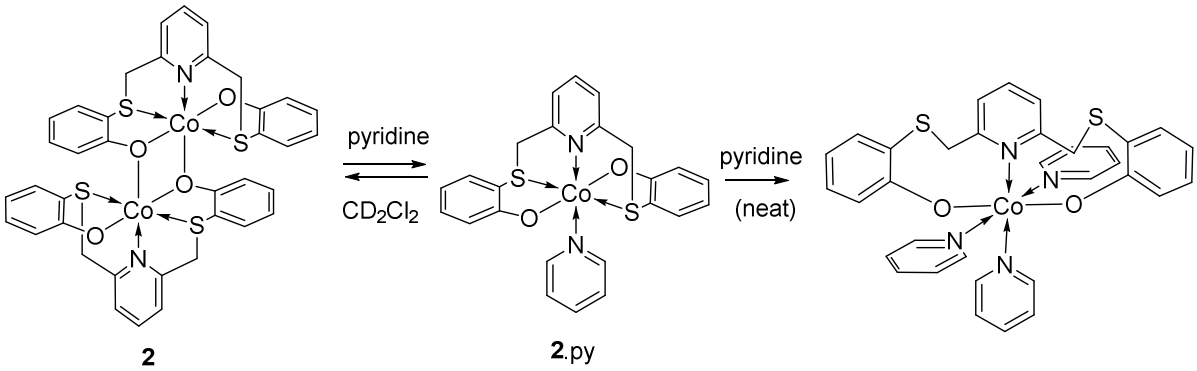

Scheme 3. Equilibria between complex **2** and its pyridine adducts.

The yellow powder isolated by precipitation from a solution of compound **2** in neat pyridine was characterized by elemental analysis, ESI-MS, FT-IR and UV-Vis, supporting the formation the mono-adduct **2**·py (see experimental section and ESI – Figure S4 and S14). Slow diffusion of pentane into a saturated pyridine solution of **2** afforded dark single crystals suitable for X-ray diffraction analysis. The solid-state structure, depicted in Figure 4, confirmed the formation of the mono-pyridine adduct **2**·py under these conditions. The complex adopts a distorted octahedral geometry around the cobalt(II) center. Ligand **1** acts as a pentadentate tetrapodal ligand, with the two thioether-phenolate (S,O) moieties oriented *anti* to each other, and the connecting pyridine (of **1**) located *trans* to the additional pyridine ligand. A similar ligand arrangement was observed in the case of a closely related pyridine adduct of a OSNSO-copper(II) complex [40]. As expected, the Co-L (L = donor atom) bond lengths respect the following order: Co-O [2.009(3) Å] < Co-N [2.150(5) Å for N2 and 2.165(5) Å for N1] < Co-S [2.4502(11) Å] (see ESI – Table S2 for the list of bond lengths and angles for **2**·py). The bite angle values of the *S,O*- and *S,N*-chelates are 84.44(9)° and 81.85(3)°, respectively, and the other angles around the Co^{II} center were found in the range 89.40(8)- 98.15(3)°. No X-ray structure of other cobalt complexes with a coordination sphere composed of two phenolate, two thioether and two pyridine donors are available for comparison. However, the structural parameters of complex **2**·py could be compared to other cobalt(II) complexes presenting an $O_2S_2N_2$ coordination sphere, with O = phenolate, alkoxide or carboxylate, S = thioether and N = pyridyl or neutral amine donors [58-60]. The ranges of the Co-O [1.952(3)-2.033(2) Å], Co-N [2.134(3)-2.198(3) Å] and Co-S [2.478(2)-2.657(1) Å] bond lengths in these compounds encompass those observed for **2**·py (see above).

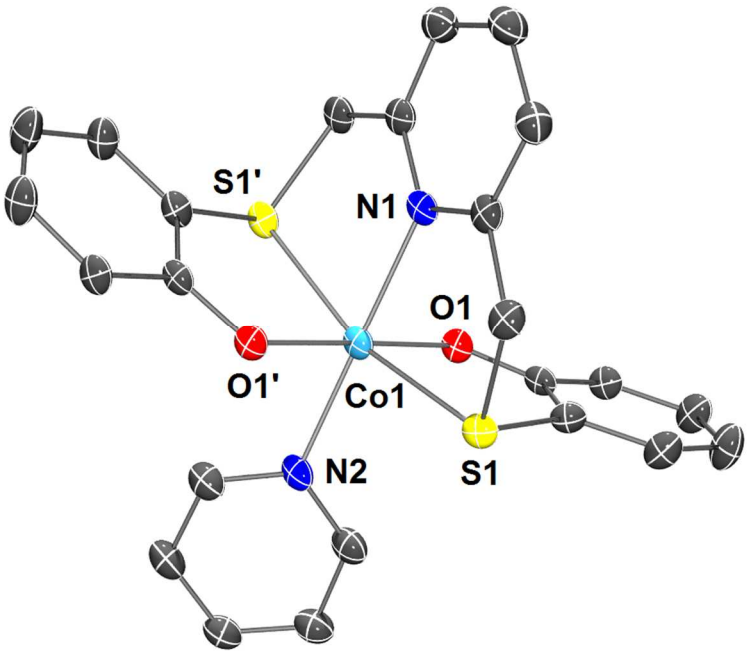

Figure 4. View of the molecular structure of **2**·py with ellipsoids set at the 50% probability level. H atoms omitted for clarity. Symmetry code: (') -x+1,y,-z+1/2. Selected bond lengths (Å) and angles (deg.): Co1-O1 2.009(3), Co1-N1 2.165(5), Co1-N2 2.150(5), Co1-S1 2.4502(11), O1-Co1-O1' 178.80(17), O1-Co1-N1 90.60(8), O1-Co1-N2 89.40(8), O1-Co1-S1 95.73(9), N1-Co1-N2 180.0, N1-Co1-S1 81.85(3), N2-Co1-S1 98.15(3), S1-Co1-S1' 163.70(6).

The ^{1}H NMR spectrum obtained for a solution of **2** in neat d_5-pyridine (see Exp. section and ESI – Figure S5), on the other hand, is different from that observed in CD_2Cl_2 at high py/Co ratio. In addition to the residual solvent resonances, seven resonances are clearly shown with approximate relative intensity 2:2:2:2:4:1:2. This is consistent with the number of different protons in the ligand in C_{2v} symmetry, whereas the C_2 symmetry observed in the solid state would predict a larger number of resonances. In particular, the methylene protons in the CH_2S tether should be diastereotopic, thus no resonance with a relative intensity corresponding to 4 protons should be present. This suggest the presence of yet another equilibrium, resulting in the decoordination of the labile sulfur donors and generation of a tris(pyridine) adduct in the presence of a large pyridine concentration, as suggested in Scheme 3. Very small resonances corresponding to those observed in neat d_5-pyridine could indeed be detected also in the CD_2Cl_2 solutions at high py/Co ratios, by a fuller exploration of this pyridine addition equilibrium was not carried out.

The species present in pyridine solution was EPR silent down to liquid nitrogen temperature, but a spectrum could be detected at 4.13 K (ESI – Figure S6). It exhibits a characteristic signal for a cobalt(II) species with a tetragonal g-tensor ($g_{\perp}$ = 5.00 and $g_{||}$ = 3.88) and hyperfine coupling that could not be properly modelled [61, 62]. Indeed, the expected eight lines signal, corresponding to ^{59}Co (I = 7/2) hyperfine splitting, may be further split into five lines due to the coupling with the two *trans*-coordinated pyridine nitrogen atoms [61].

No cyclic voltammetric (CV) data could be obtained for complexes **2** and **2**·py in pure dichloromethane (DCM) nor acetonitrile due to their extremely low solubility in these solvents. Therefore, the CV analyses were performed in DCM with addition of 8 µL of pyridine, in order to solubilize the complexes. Under these conditions, the cyclic voltammograms of **2** and **2**·py were found very similar, exhibiting a reversible redox wave at $E_{1/2}$ = 0.071 and 0.064 V vs SCE, respectively, and with separations between the anodic and cathodic peaks of 0.074 and 0.103 V respectively, which could be assigned to the cobalt(II)/cobalt(III) redox couple (Figure 5) [61].

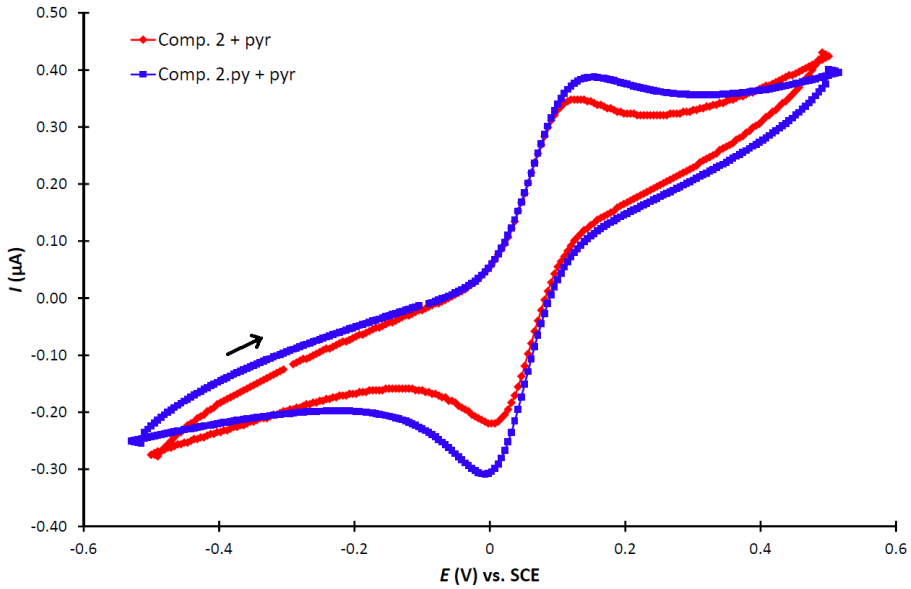

Figure 5. Cyclic voltammograms of complex **2** (red) and **2**·py (blue) in dry CH_2Cl_2 (1 mM) with addition of 8µL of pyridine, at a scan rate of 200 mV s^{-1}.

2.3. Synthesis of the cobalt(III) complexes 3 and 4

The cobalt(II) center of complex **2** could be smoothly and selectively oxidized to cobalt(III) by reaction with iodine (Co/I_2 1:0.5 molar ratio) in MeOH (Scheme 4, top). The cobalt(III) iodide complex **3** was isolated in good yields (77%) and characterized by ^1H and $^{13}C\{^1H\}$ NMR, FT-IR, ESI-MS, UV-Vis and EA. The NMR analyses confirmed the diamagnetic nature of the compound (d^6 configuration). In d_6-DMSO, the chemical shift of the signal attributed to the CH_2 groups (4H) is downfield shifted by *ca*. 1 ppm from the position found for the free ligand, (ESI – compare Figures S7 and S1) and the ^{13}C NMR signal of the same CH_2 group is also strongly downfield shifted to 55.6 ppm in **3** vs. 37.5 ppm in **1**·H_2 (ESI – compare Figures S8 and S2). Notably, the CH_2 protons resonate as a second-order AB system (^2J = 17 Hz) confirming the κ^5-coordination mode of ligand **1** and formation of a stereogenic sulfur center upon coordination. In $CDCl_3$, the diastereotopic methylene H atoms are more greatly separated, yielding an AX spin system centered at 4.73 and 5.19 ppm with a ^2J of 19 Hz (ESI – Figures S9)[63]. The signals of the aromatic H, on the other hand, are only slightly affected by the coordination process. The UV-Vis spectrum of complex **3** , in CH_2Cl_2, revealed an intense absorption band centered at 417 nm, along with a shoulder around 535 nm (see ESI – Figure S14). Despite numerous attempts, no crystals of **3**, suitable for an X-ray diffraction analysis, could be grown.

Compound **3** could further be engaged in an halide abstraction reaction, using an equimolar amount of $KB(C_6F_5)_4$ in dichloromethane at room temperature (Scheme 4, bottom). The resulting cationic complex **4** could be isolated in good yields (90%) and characterized by various spectroscopic and analytical techniques (see Exp. Section and ESI). The ^1H NMR spectrum of complex **4** in d_6-acetone (Figures S10) resembles that of its precursor **3** (ESI – Figures S11), nevertheless both signals of the CH_2 linkers (δ 5.03 (**4**) and 5.15 (**3**) ppm) and the *para*-H of the pyridyl groups (δ 7.91 (**4**) and 7.80 (**3**) ppm) were significantly shifted. Both $^{19}F\{^1H\}$ and $^{11}B\{^1H\}$ NMR spectra confirmed the presence of the $B(C_6F_5)_4$ counter ion and the absence of any cation-anion interaction (ESI – Figures S12 and S13) [64, 65]. The formation of **4** from **3** was accompanied by a shift of the strong absorption band in the UV-Vis spectrum (in CH_2Cl_2) from 417 to 401 nm and by the disappearance of the shoulder at 535 nm (see ESI – Figure S14). To the best of our knowledge, no example of cationic pentacoordinated (OSNSO)-cobalt(III) complexes were reported. However, several examples of six-coordinated cationic cobalt(III) complexes, supported by one (hexadentate) or two (tridentate) related ligands based of N, S, and O-

donors were structurally characterized [66-69]. It is therefore reasonable to speculate that compound **4** exists more likely as an O- or S-bridged dimeric species or as solvent adduct in coordinating solvents, such as acetone.

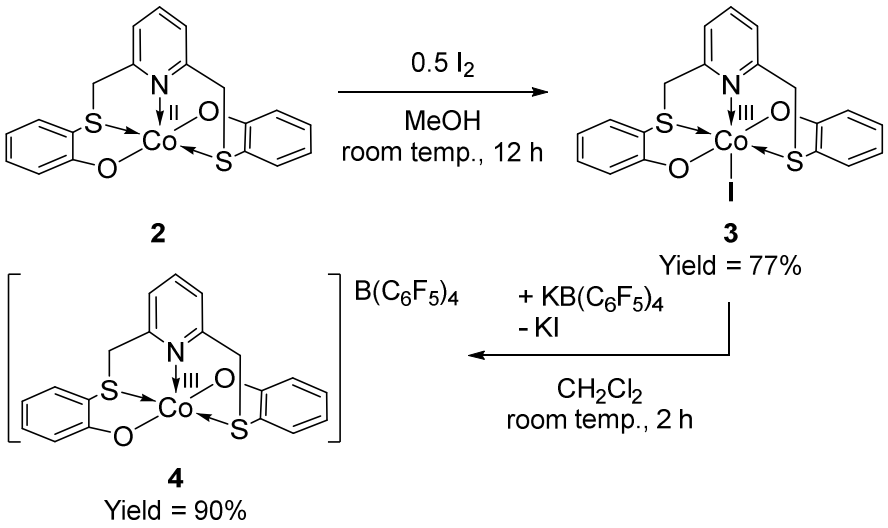

Scheme 4. Oxidation of the cobalt(II) complex **2** to the cobalt(III) iodo complex **3** (top) and formation of the cationic complex **4** by halide abstraction (bottom).

2.4. Polymerization tests

Complexes **2** and **2**·py were evaluated as moderators in radical polymerization of styrene, *tert*-butyl acrylate and vinyl acetate under various reaction conditions, but in all cases no control of the polymerization was observed (see ESI – Table S4 for details). The polymerization kinetics were similar to that of the free radical polymerization (absence of cobalt), meaning that the presence of the cobalt complex did not provide efficient trapping of the active radical species. Moreover, the recovered polymer samples exhibited much higher molecular weights (MW) than expected for a controlled process and broad dispersities. The lack of control was attributed to the non-solubility of **2** in pure monomer and to the competition between radical trapping and Lewis base coordination under homogeneous conditions, the latter being achieved only in the presence of 90 (at 80°C) or 330 (at 65°C) equiv pyridine.

3. Conclusion

In the present study, we reported the synthesis of a new OSNSO-tetrapodal pentadentate proligand and its complete characterization, including by X-ray crystallography, as a potential alternative to salen/salan/salalen ligands for applications in cobalt mediated radical polymerization. The corresponding cobalt(II) complex **2** was obtained via a one-step procedure in high yield. CV studies confirmed that the required (for OMRP) Co^{II}/Co^{III} couple is accessible with this ligand. Unfortunately, the poor solubility of **2** prevented any control of radical polymerization processes. The reactivity of complex **2** was further investigated, establishing that it has a high affinity towards Lewis bases, such as pyridine, and the mono-pyridine adduct **2**·py could be isolated and characterized, including via paramagnetic ^{1}H NMR and X-ray crystallography. Complex **2** was cleanly oxidized to its iodo cobalt(III) analog **3** and the latter could then be subjected to an halide abstraction reaction, affording the cationic complex **4** in high yield. The high-valent complexes **3** and **4** may be of interest for further applications in ring-opening copolymerization of CO_2 and epoxides for the production of polycarbonates, as their salen analogs. Ligand modifications are currently under investigation, in order to improve the solubility of the resulting complexes.

4. Conflict of interest

The authors declare no conflict of interest.

5. Acknowledgements

The authors thank the Centre National de la Recherche Scientifique (CNRS, France) and the Ministère de l'Enseignement Supérieur, de la Recherche et de l'Innovation, France (Ph.D. fellowship to L.T.) for support of this work. Alix Sournia-Saquet and Lionel Rechignat are gratefully acknowledged for the CV and EPR measurements, respectively.

6. Appendix A. Supplementary data

NMR spectra of compounds **1**·H_2, **2**·py, **3** and **4**; ESI-MS spectra of complex **2** and **2**·py; UV-Vis spectra of complexes **2**·py, **3** and **4**; EPR spectrum of **2**·py; details about the study of the equilibrium between complex **2** and the pyridine adduct **2**·py; tables summarizing all bond lengths, angles and hydrogen interactions in the solid-state structures of compounds **1**·H_2 and **2**·py are available in the Electronic Supporting Information.

7. References

[1] M. Hapke, G. Hilt, Cobalt catalysis in organic synthesis: Methods and reactions, Wiley-VCH Verlag GmbH & Co. KGaA, Weinheim, Germany, 2020.
[2] R.J.M. Klein Gebbink, M.-E. Moret, Non-noble metal catalysis: Molecular approaches and reactions, Wiley-VCH Verlag GmbH & Co. KGaA, Weinheim, Germany, 2019.
[3] H. Wen, G. Liu, Z. Huang, Coord. Chem. Rev., 386 (2019) 138-153.
[4] D. Wei, C. Darcel, Chem. Rev., 119 (2019) 2550-2610.
[5] L. Alig, M. Fritz, S. Schneider, Chem. Rev., 119 (2019) 2681-2751.
[6] W. Liu, B. Sahoo, K. Junge, M. Beller, Acc. Chem. Res., 51 (2018) 1858-1869.
[7] S. Dadashi-Silab, K. Matyjaszewski, Molecules, 25 (2020) 1648.
[8] Z. Xue, D. He, X. Xie, Polym. Chem., 6 (2015) 1660-1687.
[9] R. Poli, L.E.N. Allan, M.P. Shaver, Prog. Polym. Sci., 39 (2014) 1827-1845.
[10] C. Fliedel, R. Poli, J. Organomet. Chem., 880 (2019) 241-252.
[11] J. Demarteau, A. Debuigne, C. Detrembleur, Chem. Rev., 119 (2019) 6906-6955.
[12] A. Debuigne, C. Jérôme, C. Detrembleur, Polymer, 115 (2017) 285-307.
[13] R. Poli, Chem. Eur. J., 21 (2015) 6988-7001.
[14] L.E.N. Allan, M.R. Perry, M.P. Shaver, Prog. Polym. Sci., 37 (2012) 127-156.
[15] M. Hurtgen, C. Detrembleur, C. Jerome, A. Debuigne, Polym. Rev., 51 (2011) 188-213.
[16] A. Debuigne, R. Poli, C. Jerome, R. Jerome, C. Detrembleur, Prog. Polym. Sci., 34 (2009) 211-239.
[17] L. Thevenin, C. Fliedel, K. Matyjaszewski, R. Poli, Eur. J. Inorg. Chem., 2019 (2019) 4489-4499.
[18] M. Fantin, F. Lorandi, T.G. Ribelli, G. Szczepaniak, A.E. Enciso, C. Fliedel, L. Thevenin, A.A. Isse, R. Poli, K. Matyjaszewski, Macromolecules, 52 (2019) 4079-4090.
[19] R. Poli, Eur. J. Inorg. Chem., (2011) 1513-1530.
[20] R. Poli, Angew. Chem. Int. Ed., 45 (2006) 5058-5070.
[21] J. Wang, X. Xie, Z. Xue, C. Fliedel, R. Poli, Polym. Chem., 11 (2020) 1375-1385.
[22] J. Wang, J. Han, X. Xie, Z. Xue, C. Fliedel, R. Poli, Macromolecules, 52 (2019) 5366-5376.
[23] J. Wang, J. Han, H. Peng, X. Tang, J. Zhu, R.-Z. Liao, X. Xie, Z. Xue, C. Fliedel, R. Poli, Polym. Chem., 10 (2019) 2376-2386.
[24] R. Morales-Cerrada, V. Ladmiral, F. Gayet, C. Fliedel, R. Poli, B. Ameduri, Polymers, 12 (2020).
[25] R. Morales-Cerrada, C. Fliedel, J.C. Daran, F. Gayet, V. Ladmiral, B. Ameduri, R. Poli, Chem. Eur. J., 25 (2019) 296-308.
[26] Y.K. Redjel, L. Thevenin, J.-C. Daran, M. Benslimane, R. Poli, C. Fliedel, Polyhedron, 158 (2019) 83-90.

[27] S. Banerjee, V. Ladmiral, A. Debuigne, C. Detrembleur, R. Poli, B.M. Ameduri, Angew. Chem. Int. Ed., 57 (2018) 2934-2937.
[28] E.V. Bellan, L. Thevenin, F. Gayet, C. Fliedel, R. Poli, ACS Macro Lett., 6 (2017) 959-962.
[29] Z. Wang, R. Poli, C. Detrembleur, A. Debuigne, Macromolecules, 52 (2019) 8976-8988.
[30] P.G. Falireas, V. Ladmiral, A. Debuigne, C. Detrembleur, R. Poli, B. Ameduri, Macromolecules, 52 (2019) 1266-1276.
[31] S. Banerjee, V. Ladmiral, A. Debuigne, C. Detrembleur, S.M.W. Rahaman, R. Poli, B. Améduri, Macromol. Rapid Commun., 38 (2017) 1700203.
[32] S. Banerjee, E.V. Bellan, F. Gayet, A. Debuigne, C. Detrembleur, R. Poli, B. Améduri, V. Ladmiral, Polymers, 9 (2017) 702.
[33] A.N. Morin, C. Detrembleur, C. Jerome, P. De Tullio, R. Poli, A. Debuigne, Macromolecules, 46 (2013) 4303-4312.
[34] F.-S. Wang, T.-Y. Yang, C.-C. Hsu, Y.-J. Chen, M.-H. Li, Y.-J. Hsu, M.-C. Chuang, C.-H. Peng, Macromol. Chem. Phys., 217 (2016) 422-432.
[35] C.H. Peng, T.Y. Yang, Y. Zhao, X. Fu, Org. Biomol. Chem., 12 (2014) 8580-8587.
[36] R. Poli, S.M.W. Rahaman, V. Ladmiral, B. Ameduri, J. Organomet. Chem., 864 (2018) 12-18.
[37] A. Debuigne, A.N. Morin, A. Kermagoret, Y. Piette, C. Detrembleur, C. Jerome, R. Poli, Chem. Eur. J., 18 (2012) 12834-12844.
[38] Y. Champouret, K.C. MacLeod, U. Baisch, B.O. Patrick, K.M. Smith, R. Poli, Organometallics, 29 (2010) 167-176.
[39] A. Debuigne, Y. Champouret, R. Jerome, R. Poli, C. Detrembleur, Chem. Eur. J., 14 (2008) 4046-4059.
[40] R.C. Pratt, L.M. Mirica, T.D.P. Stack, Inorg. Chem., 43 (2004) 8030-8039.
[41] S. Maria, H. Kaneyoshi, K. Matyjaszewski, R. Poli, Chem. Eur. J., 13 (2007) 2480-2492.
[42] B. Rezzonico, M.J. Grigon-Dubois, J. Chem. Res. (S), (1994) 142-143.
[43] G.M. Sheldrick, Acta Crystallogr. Sect. A: Found. Crystallogr., A71 (2015) 3-8.
[44] G.M. Sheldrick, Acta Crystallogr. Sect. C: Cryst. Struct. Commun., C71 (2014) 3-8.
[45] A.L. Spek, Acta Crystallogr. Sect. C: Cryst. Struct. Commun., C71 (2015) 9-18.
[46] F.L. J., J. Appl. Crystallogr., 30 (1997) 565-565.
[47] M.N. Burnett, C.K. Johnson, Report ORNL-6895. Oak Ridge National Laboratory, Tennessee, USA, (1996).
[48] L.C. Song, X.J. Sun, P.H. Zhao, J.P. Li, H.B. Song, Dalton Trans., 41 (2012) 8941-8950.
[49] M. Al-Noaimi, R.J. Crutchley, M. AlDamen, A.M. Rawashdeh, M.A. Khanfar, K. Seppelt, Polyhedron, 30 (2011) 2075-2082.
[50] F. Teixidor, P. Anglès, C. Viñas, R. Kivekäs, R. Sillanpää, Inorg. Chem., 40 (2001) 4010-4015.
[51] R. Sillanpää, R. Kivekäs, L. Escriche, G. Sánchez-Castelló, F. Teixidor, Acta Crystallogr. Sect. C: Cryst. Struct. Commun., C50 (1994) 1284-1286.
[52] Y.-C. Su, C.-Y. Tsai, L.-S. Huang, C.-H. Lin, B.-T. Ko, Dalton Trans., 48 (2019) 12239-12249
[53] M. Fondo, J. Doejo, A.M. García-Deibe, J. Sanmartín-Matalobos, R. Vicente, M.S. El-Fallah, M. Amoza, E. Ruiz, Inorg. Chem., 55 (2016) 11707-11715.
[54] S. Jie, P. Ai, B.-G. Li, Dalton Trans., 40 (2011) 10975-10982
[55] I.A. Koval, M. Huisman, A.F. Stassen, P. Gamez, M. Lutz, A.L. Spek, D. Pursche, B. Krebs, J. Reedijk, Inorg. Chim. Acta, 357 (2004) 294-300.
[56] D. Black, A.J. Blake, K.P. Dancey, A. Harrison, M. McPartlin, S. Parsons, P.A. Tasker, G. Whittaker, M. Schröder, J. Chem. Soc., Dalton Trans., (1998) 3953-3960
[57] A.J. Blake, L.M. Gilby, S. Parsons, J.M. Rawson, D. Reed, G.A. Solan, R.E.P. Winpenny, J. Chem. Soc., Dalton Trans., (1996) 3575-3581.
[58] J.A. Denny, W.S. Foley, A.D. Todd, M.Y. Darensbourg, Chem Sci, 6 (2015) 7079-7088.
[59] A.A. Dar, S. Hussain, D. Dutta, P.K. Iyer, A.T. Khan, RSC Advances, 5 (2015) 57749-57756.
[60] R. Mattes, T. Entian, Z. Anorg. Allg. Chem., 629 (2003) 2298-2304.
[61] A. Pui, C. Policar, J.-P. Mahy, Inorg. Chim. Acta, 360 (2007) 2139-2144.
[62] S.J. Dzugan, D.H. Busch, Inorg. Chem., 29 (1990) 2528-2532.

[63] H. Pellissier, Chiral sulfur ligands: Asymmetric catalysis, Royal Society of Chemistry, 2009.
[64] D. Specklin, F. Hild, C. Fliedel, C. Gourlaouen, L.F. Veiros, S. Dagorne, Chem. Eur. J., 23 (2017) 15908 – 15912.
[65] D. Specklin, C. Fliedel, C. Gourlaouen, J.C. Bruyere, T. Aviles, C. Boudon, L. Ruhlmann, S. Dagorne, Chem. Eur. J., 23 (2017) 5509-5519.
[66] A.K. Ghosh, C.S. Purohit, R. Ghosh, Polyhedron, 155 (2018) 194-201.
[67] P. Pattanayak, J.L. Pratihar, D. Patra, C.-H. Lin, S. Paul, K. Chakraborty, Polyhedron, 51 (2013) 275-282.
[68] C.R. Lucas, J.M.D. Byrne, J.L. Collins, L.N. Dawe, D.O. Miller, Can. J. Chem., 89 (2011) 1174-1189.
[69] P. Chakraborty, S.K. Chandra, A. Chakravorty, Inorg. Chem., 33 (1994) 4959-4965.